Man-Portable Dense Plasma Focus for Neutron Interrogation Applications

NLV-009-17 | Year 3 of 3

Brady Gall,[1,a] Michael Heika,[a] Michael Blasco,[a] Joseph Bellow,[a] Bernard T. Meehan,[a] James Tinsley,[b] Mark Gerling,[c] Nichelle Bennett,[c] Jessie Walker,[d] Yuri Podpaly,[e] and Steven Chapman[e]

[1]gallbb@nv.doe.gov, (702) 295-3117
[a]Nevada Operations; [b]Special Technologies Laboratory; [c]Sandia National Laboratories; [d]Los Alamos National Laboratory, [e]Lawrence Livermore National Laboratory

Over the last three years, a portable, high-output dense plasma (DPF) focus system was designed, constructed, and tested in support of Threat Reduction Science and Technology's active interrogation applications. This work culminated in an experimental series to measure active fission products from nuclear materials using signal from the portable DPF in a multi-lab collaboration with teams from the Nevada National Security Site (NNSS), Sandia (SNL), Lawrence Livermore (LLNL), and Los Alamos national laboratories. Our transportable DPF system has a simple operating platform and produces up to 1×10^8 neutrons per pulse using pure deuterium fuel with a repetition rate of two shots per minute. Experimental facilities used in this effort included the NNSS's Radiological/Nuclear Countermeasures Test and Evaluation Complex (RNCTec), where we measured signal from depleted uranium, and the Device Assembly Facility (DAF), where we measured signal from highly enriched uranium. Diagnostics included SNL's Mobile Imager of Neutrons for Emergency Responders (MINER) imaging system and LLNL's recently developed fast-fission detector array. Depleted uranium was detectable with high certainty, but logistical complications limited our ability to collect data on highly enriched uranium, so results from this material are inconclusive. This project has demonstrated that portable DPF systems can be used to detect nuclear material and established administrative pathways to enable future interrogations at NNSS facilities using DPF platforms.

Background

The dense plasma focus (DPF) device has long been considered an inexpensive, compact, pulsed neutron source (Mather 1964, 1965; Bernard 1977), and it is currently being explored for a range of applications from activation analysis and plasma nanotechnology to radiography and material detection (Gribkov 2006, Zhang 2007, Hussain 2010, Krishnan 2012, Rawat 2013). Recent DPF development has focused on increasing the device's portability and pulse repetition rates (Lee 1998, Rapezzi 2004, Shukla 2015, Niranjan 2016). The goal of this project was to leverage these advances in portable pulsed-power technology, along with existing expertise in large-scale DPF systems at the NNSS, to build a new, compact device capable of meeting the needs of nuclear search, warhead confirmation and monitoring, and render safe (Office of Defense Nuclear Nonproliferation 2018) applications in which objects suspected to contain special nuclear material (SNM) are inspected by gamma or neutron radiation fields. By examining the response products emitted from the object, we may ascertain its internal composition and configuration. For many reasons, it is not practical for test objects to be shipped from multiple locations to a central location for inspection. Instead, we need a reliable, high-flux neutron source that can be brought to the object's location. According to a needs survey prepared in 2016, the source must produce at least 10^6 neutrons per second, be reasonably portable and rugged, and be simple to operate. Such a source would enable us to accomplish these mobile applications.

Compact neutron source technology is a mature field of research, and many options are available commercially. Some systems, such as the Adelphi DT108API, operate in continuous mode, while others, such as the Thermo Scientific MP 320, produce microsecond-scale bursts of neutrons at a high repetition rate. Both continuous and pulsed modalities can be used for SNM

detection, but pulsed sources offer additional functionality; of special interest to us is their ability to measure delayed gamma and neutron products from fission multiplication, which augments the capability of an SNM-sensing platform. Short pulses turn off quickly, providing a low-background time window to detect the delayed products. Additionally, Lawrence Livermore National Laboratory's (LLNL) fast-fission diagnostic method requires a neutron pulse on the order of ten nanoseconds, and it is therefore incompatible with commercially available neutron generators. The DPF can produce pulses up to 10,000 times shorter than the MP 320 neutron generator and maintain a comparable time-average neutron flux. DPF systems can be made quite compact, enabling mobile operation. With the ability to generate high-amplitude, short-pulse-width neutron fields in a readily transportable form factor, DPF technology is an ideal candidate for portable active interrogation applications.

Project

This project was a three-year investigation to design and build a portable DPF for defense nuclear nonproliferation applications. In year one, we designed a new DPF plasma source geometry, procured compact high-voltage hardware, developed control system software, and assembled and tested a tabletop pulsed power driver (Gall 2018). In year two, we fabricated the new DPF plasma source, shrunk the tabletop pulsed-power driver, coupled the DPF to the pulsed-power driver, and tested the integrated system for neutron production. The result was a successful and repeatable demonstration of neutron output with an average yield of 2.5×10^7 neutrons per pulse and a pulse width of approximately 30 ns FWHM (Gall 2019). In the third and final year of the project, we greatly reduced the total size of the DPF control system by

incorporating it into a portable test stand, improved the shot-to-shot repeatability and overall yield of the neutron source, and fielded the DPF at experimental facilities to expose SNM objects to neutron fields and measure the target response products.

This report describes the work we completed in FY 2019. An overview of the basic principles of the DPF is presented, followed by a description of the mechanical design of the pulsed-power driver and plasma source. We next detail experimental configuration and diagnostics used to measure the electrical and radiological output of the DPF and the experimental results. Finally, we discuss results from the experimental campaigns at the Radiological/Nuclear Countermeasures Test and Evaluation Complex (RNCTec) and the Device Assembly Facility (DAF) to measure SNM response products.

Dense Plasma Focus Operational Principle

The DPF device is a coaxial accelerator with a blunt anode termination that is filled with a low-density gas, typically pure deuterium or a deuterium-tritium mixture. As the accelerator is pulsed, the gas is ionized and accelerated through the $\mathbf{J} \times \mathbf{B}$ force to the end of the anode. The plasma pinches at the anode tip with sufficient velocity to create neutrons by fusion processes. DPF operation occurs in four phases, as shown in Figure 1. The gas ionizes in the first phase with the arrival of a high-voltage pulse. This phase is called the gas-breakdown phase. The conductivity increases rapidly as the current-carrying plasma sheath is formed. As the current rises and the $\mathbf{J} \times \mathbf{B}$ force increases, the plasma sheath is accelerated to the end of the anode. This second phase is referred to as the run-down phase. The third phase, or the run-in phase, occurs after the plasma sheath reaches the end of the anode and is accelerated radially inward. The

fourth phase is the pinch phase, where the plasma densities and temperatures (energies) have increased sufficiently to enable fusion reactions.

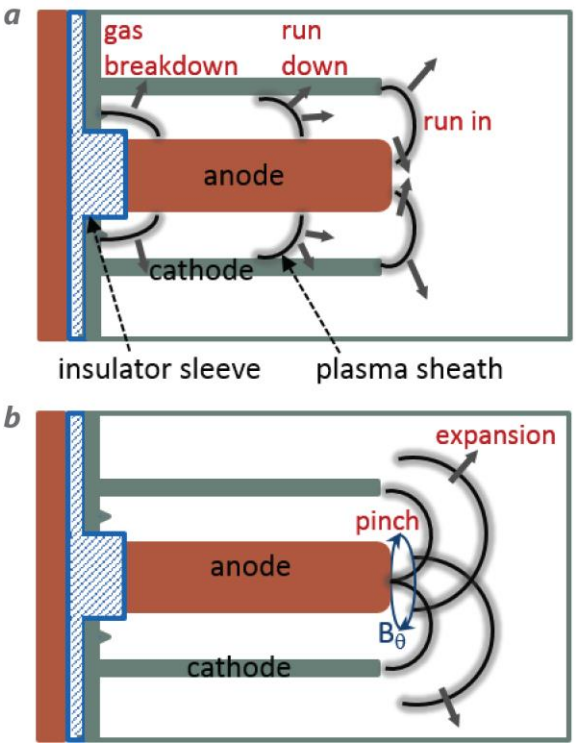

Figure 1. The DPF operation phases. During the gas-breakdown phase, the voltage pulse is injected through the insulator sleeve (blue), and a plasma sheath (black) is formed between the anode tube (brown) and the cylindrical cathode (gray). This sheath is accelerated axially during the run-down phase and radially during the run-in phase. After the pinch phase, the plasma expands radially and axially to the outer cathode.

Design of the Portable Dense Plasma Focus

The dimensions and geometry of the DPF anode and cathode geometry were designed and optimized in FY 2017. The details of this design process are documented in previous years'

reports (Gall 2018, 2019). The simulations of the DPF were performed by the use of the fully relativistic electromagnetic particle-in-cell code, Chicago, which was created by the developers of LSP (Welch 2001). Many compact configurations were tested, but the top performer used a round top anode measuring 4 cm long and 1 cm in diameter, an insulator measuring 2 cm long and 2 mm thick, an anode–cathode gap measuring 1 cm, with a pressure of 6 Torr D2 and 25 kV discharge voltage; the model predicted neutron output of 1.1×10^8 neutrons per pulse.

Figure 2a shows a cross-sectional view of the coaxial anode and cathode configuration used for this experiment and Figure 2b shows a photograph of the assembled piece. This system used the dimensions determined from modeling for the top-performing design. The anode was inserted into a hollow cylinder (insulator) made from a material with high dielectric strength, such as ceramic or glass, which then was inserted into an aperture in the vacuum chamber wall. Two to three thousandths of an inch (mil) of clearance between diameters of nested components was found to be sufficient to allow for assembly. Aremco 631 high-temperature epoxy was used to create a vacuum seal between the insulator and the anode and cathode. This method was found to be superior to the previous design, which used O-rings and was prone to leaking, especially after extended use.

The vacuum chamber was a 4.5″ ConFlat flange nipple custom ordered from vacuum component vendor Kurt J. Lesker Company. A ConFlat connection on one port supported an ion beam stop formed from a copper disk implanted in a ConFlat blank to improve shot-to-shot repeatability. The second port supported the anode, cathode, and insulator. A third port was welded on to the wall of the nipple to provide vacuum and gas fill access. The anode and cathode were made of

oxygen-free copper. We tested several insulator materials, including borosilicate glass (Pyrex), glass mica (Macor), and boron nitride, but we primarily settled on alumina due to its low cost, ease of handling and manufacturing, and good high-voltage characteristics and plasma compatibility. The copper, glass, and ceramic materials were purchased from McMaster-Carr.

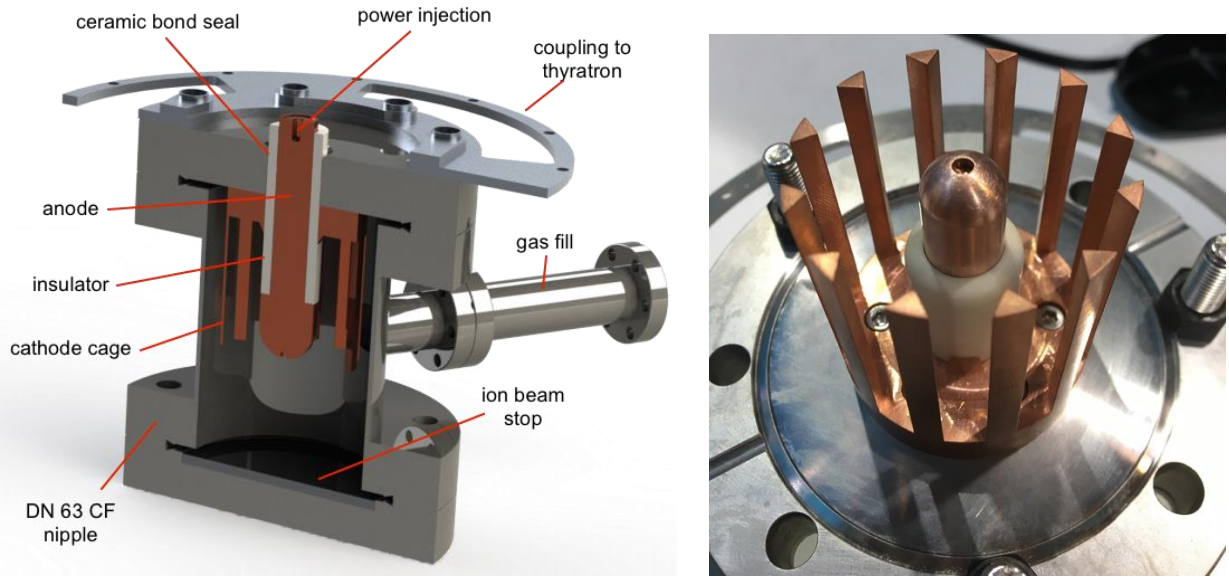

Figure 2. (left) Cutaway of DPF plasma chamber. (right) Photograph of plasma source without vacuum chamber to show anode, insulator, and cathode assembly.

Figure 3 shows a cutaway of the DPF chamber coupled to the pulsed-power driver. We used a radial arrangement of six General Atomics 31150 0.5 μF, 30 kV capacitors to drive the high-current pinch. A Pulsed Power Solutions TDI4-100k/45H cold cathode thyratron, centrally located in the capacitor bank, controlled plasma switching. To couple the DPF chamber to the thyratron, we used 1/8″ aluminum plates cut to specification with a water jet cutter.

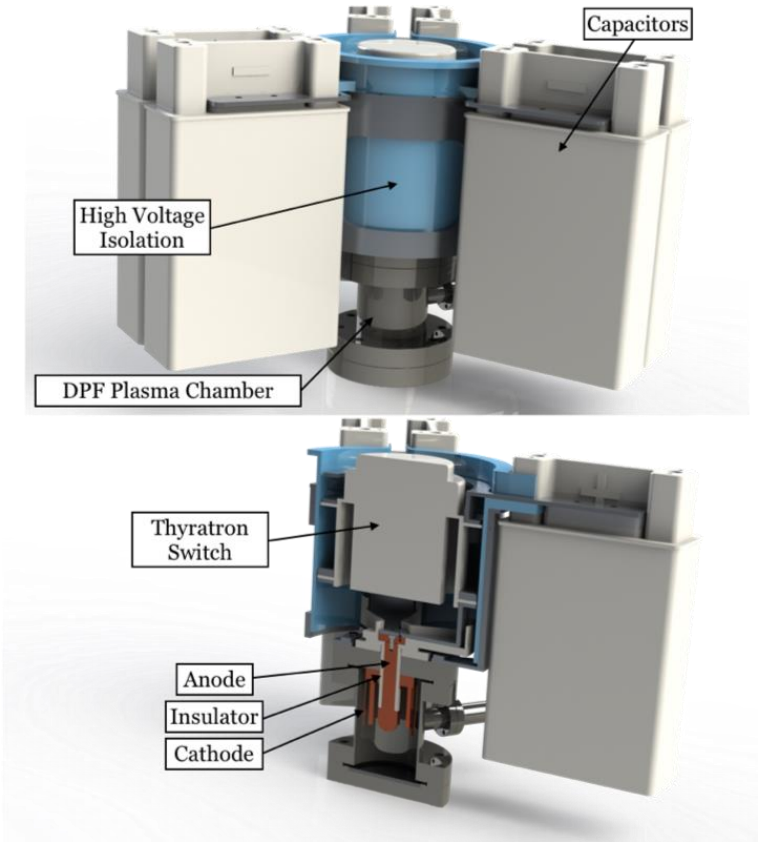

Figure 3. (top) External view of pulsed power system. (bottom) Cut-away of pulsed power system.

Previously, we used a combination of Mylar sheets, Kapton tape, and spray-on acrylic sealant to isolate our high-voltage conductors. This process was unreliable and difficult to implement. This year, we significantly upgraded the high voltage isolation on the pulsed-power system by using custom, 3D-printed acrylic insulators. We used the Formlabs Form2 3D printer and tough acrylic resin to fabricate form-fitting insulators and prevent high-voltage flashover while charging the high-voltage capacitors. This method greatly increased ease of assembly, repeatability, and reliability of the high voltage isolation. Figure 4 shows a photograph of the previous Mylar-based system compared to the newer 3D-printed method.

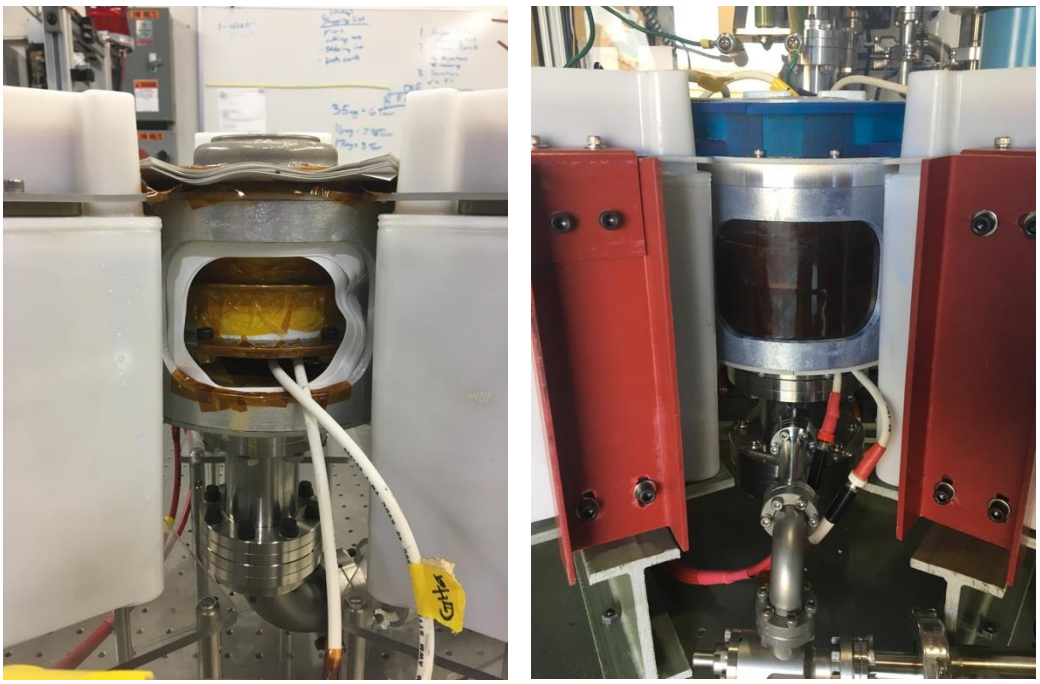

Figure 4. (left) Last year's Mylar-based high-voltage insulator. (right) Improved 3d-printed acrylic insulators. The red beams are fiberglass struts to secure the pulsed power system to the test stand frame.

The control system was also upgraded this year. The previous build, detailed in the 2018 end of year report (Gall 2019) used a LabVIEW platform to operate the DPF. This year, we used the Arduino platform to significantly reduce the cost, size, and complexity of the DPF control system. For improved survivability in high electric field environments, we used the Ruggeduino brand Arduino platform, which is specially designed to withstand static discharge, reverse current, and EMP. A simple state machine controlled an automated charging sequence and transitioned the DPF through four states: SAFE, READY, CHARGING, and FIRE. A two-key system was used to ensure that the DPF could not have stored energy unless both keys were inserted into the control panel. An emergency stop button provided additional control to allow

the operator to manually override the controller and immediately de-energize the capacitor bank. A photograph of the control panel is shown in Figure 5.

Figure 5. Control panel for portable DPF. LED indicators provide user feedback on control system status, 2-key system ensures that DPF cannot be charged accidentally, and emergency stop de-energizes capacitors through dump resistors in an off-normal event.

Figure 6 shows a block diagram of the components and interconnections of the control system and pulsed-power machine. Electrical power was provided through standard 120 VAC utility hookups, although the system could be easily adapted to 230 VAC or battery power. A Glassman MK series 75 W, 30 kV positive high-voltage power supply was used to charge the capacitor bank. The Arduino and control code monitored user input and system status to control the flow

of power to the capacitor bank and send the trigger system to the thyratron once the capacitor bank reached full charge. After receiving the trigger, the thyratron discharged into the DPF plasma source to create neutron radiation. Figure 7 shows a photograph of the assembled portable DPF system. The DPF was enclosed in a clear Plexiglas cover to prevent personnel exposure to high-voltage components and an onboard vacuum and gas handling system enabled easy pump-down and tube-filling operations. The frame was made from 1″ standard aluminum t-slotted beams; caster wheels provided mobility.

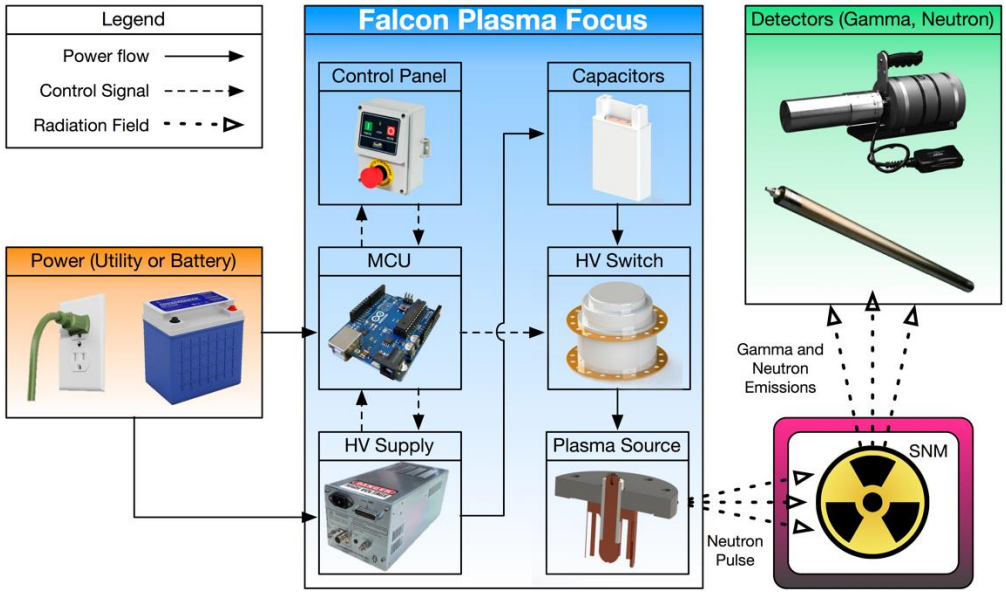

Figure 6. Block diagram showing major system components and interconnections of the portable DPF system

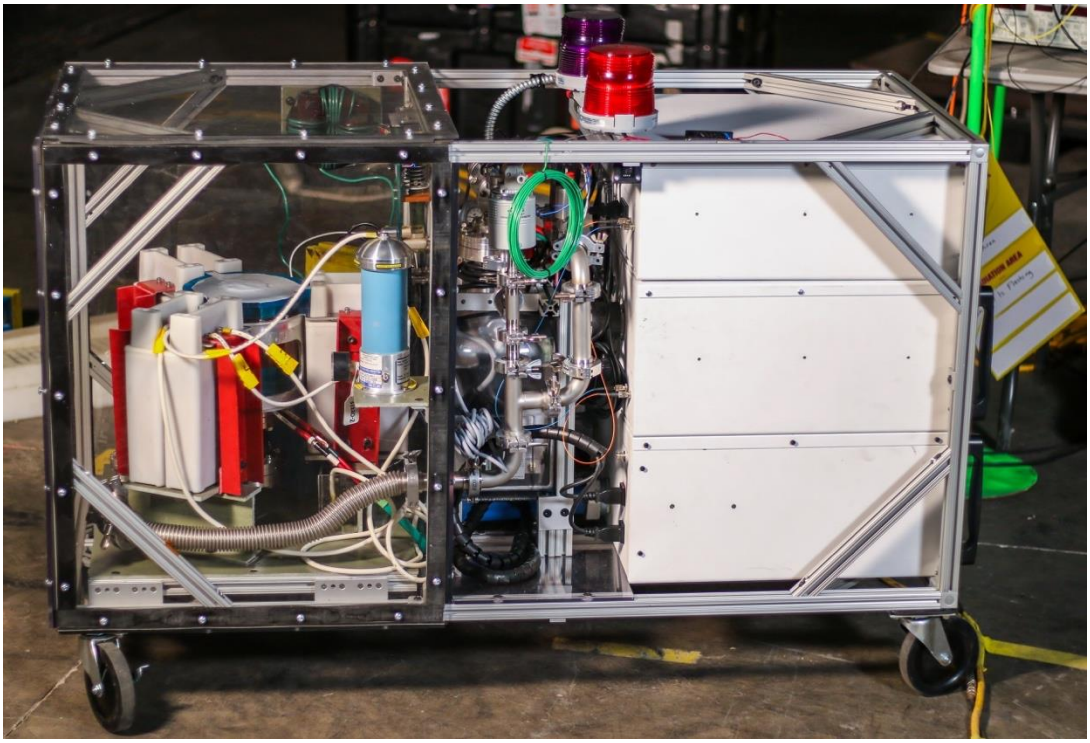

Figure 7. Photograph of assembled portable DPF system. The DPF and pulsed-power bank is on the left, the on-board vacuum system is in the center, and the control system and operator panel is on the right

DPF Performance

We used a silver activation detector developed at the Los Alamos Scientific Laboratory to quantify the neutron output of the portable DPF (Lanter 1968). The detector comprised four type 1B85 Geiger tubes wrapped with 0.01″ thick natural silver foil surrounded by a block of polyethylene moderator measuring 12″ × 12″ × 6″ and encased with galvanized steel. We calibrated this detector in-house using the 1MJ Gemini DPF located in North Las Vegas in a procedure that was detailed in the previous SDRD end of year report (Gall 2019).

In the previous section, several improvements to the DPF plasma process chamber were discussed. First, we eliminated the use of O-rings in favor of epoxy ceramic bond, which greatly improved vacuum integrity of the chamber. Second, we installed a copper plate in the ion beam path to reduce the contamination introduced to the process chamber by ion beam ablation of the stainless-steel walls. These improvements had a significant effect, which is shown in Figure 8.

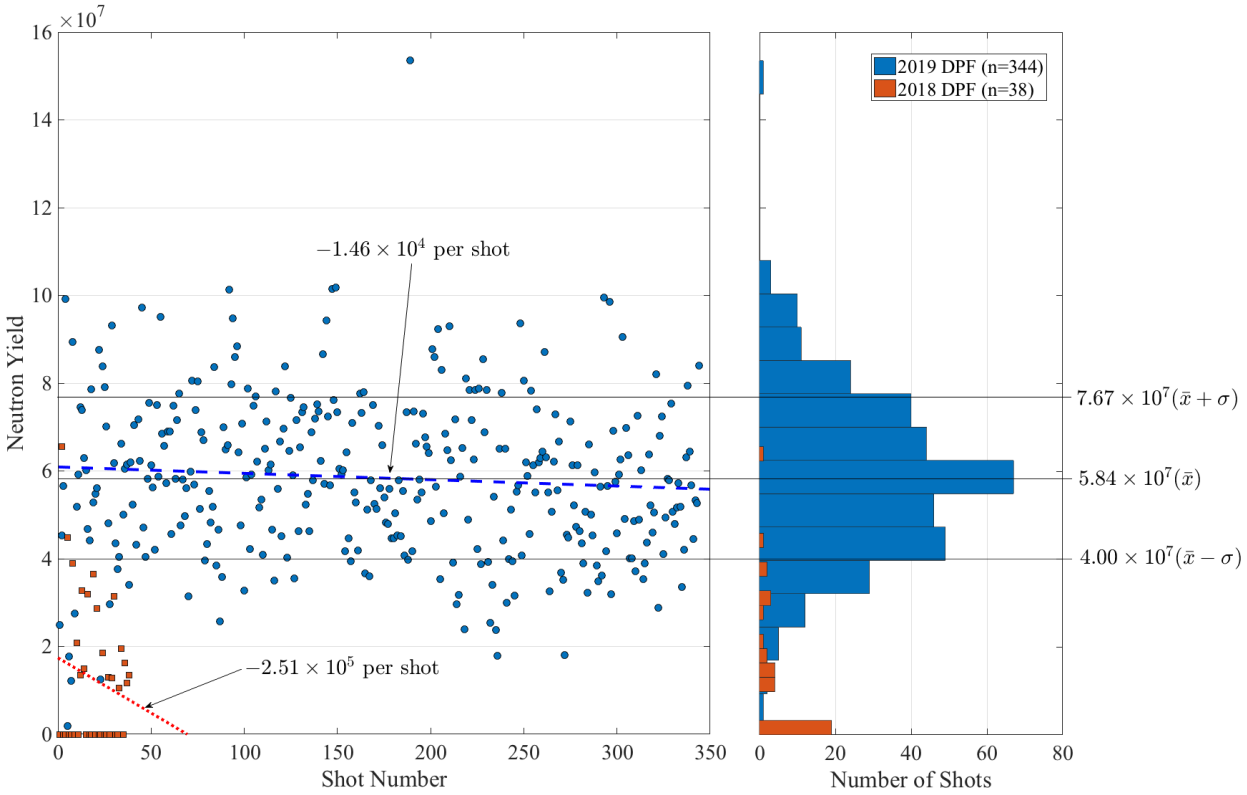

Figure 8. Neutron yield performance of 2018 and 2019 portable DPF systems. Improvements in DPF design resulted in dramatic improvement in average yield, repeatability, and longevity. Average yield = 5.84 ±1.83 × 10^7 neutrons per shot for the 2019 build.

Figure 8 shows a comparison of the neutron yield performance of the 2018 (orange) and 2019 (blue) portable DPF designs. A shot-history of the neutron yield is shown on the left and a

histogram is shown on the right. Several effects are quite clear. First, the 2019 system had much higher average yield and a much longer operational cycle. The 2018 build only produced measurable neutron yield for approximately 40 shots, whereas the 2019 build produced neutron yield up to 350 shots. Second, the 2019 build sustained its neutron yield over time, whereas the 2018 build quickly decreased in neutron yield between the beginning and the end of the shot sequence. Finally, the 2019 build produced high neutron output on every shot, but the 2018 build had zero-yield on about 50% of the shots.

The main reason for this improvement in performance was significantly higher plasma purity in the 2019 build, which was achieved by implementing the ceramic bond vacuum seal and the copper beam stop. The ceramic bond provided a much tighter vacuum seal compared to the O-ring, which experienced degradation due to the high current sustained in the power injection region of the vacuum chamber. The copper beam stop collected the ion beam and prevented non-copper metallic components from ablating within the plasma process chamber. The improvement in reliability and repeatability provided by these modifications is a significant milestone in DPF performance and makes it a compelling instrument for interrogation studies.

Figure 9 shows the gamma and neutron time-of-flight measurements for one shot on the portable DPF system, a characteristic example of a typical neutron pulse. The signal was measured using a photomultiplier tube coupled to an Eljen EJ-309 scintillator placed approximately 4 meters from the source. The first, sharper peak is from the gamma pulse generated from the DPF, and the second, wider pulse is due to the neutron field. The theoretical separation between the gamma and 2.45 MeV neutron species is 168 ns over a 4-meter drift distance that closely

matches the measured result of approximately 170 ns and is in agreement with the expected energy of the emitted neutron field. The FWHM of the neutron pulse is approximately 30 ns, which is similar to measurements made last year.

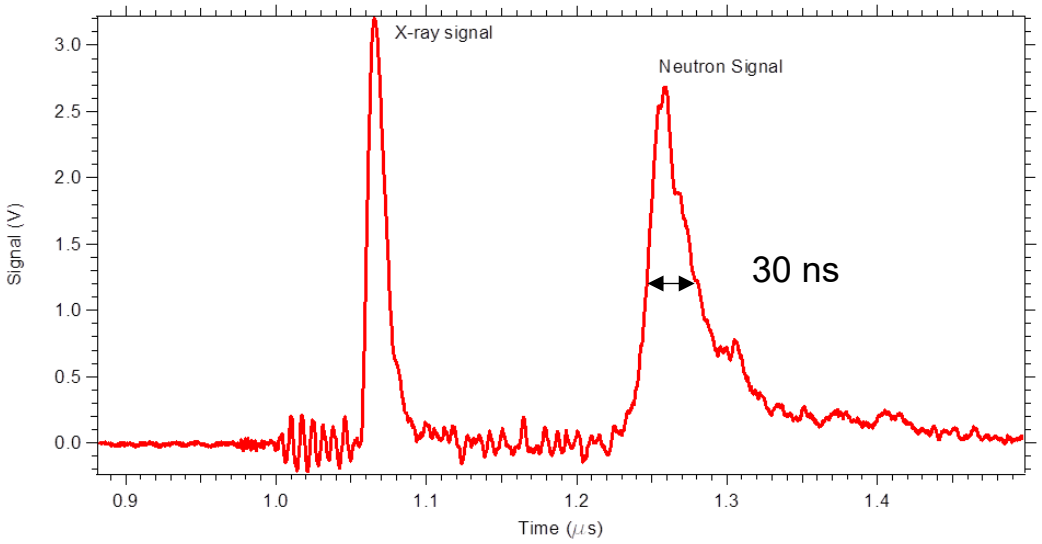

Figure 9. Time-of-flight measurements of gamma and neutron pulses from the portable DPF measured from approximately 4 meters from the source using EJ309 scintillator coupled to a photomultiplier tube

A Rogowski coil was installed at the DPF anode to measure the current of the DPF pinch. An example of a typical current waveform from a pinch is shown in Figure 10 along with a waveform predicted using the DPF simulation tool RADPF, which uses the Lee Model (Lee 2014). The Rogowski coil produces the first derivative of the DPF current, so post-processing is used to take the time-integral of the raw output and produce the waveform in Figure 10, which is current as a function of time. The measured result in orange shows that the current rises to a peak value of approximately 125 kA with a rise time of 473 ns. The time of the plasma pinch is labeled in the figure and appears as a slight dip in current, which is caused by the rapid change of

inductance from the pinch. The modeling results from RADPF were determined using the physical parameters of the portable DPF and are in generally good agreement with the experimental measurement with slight discrepancies in the pinch timing.

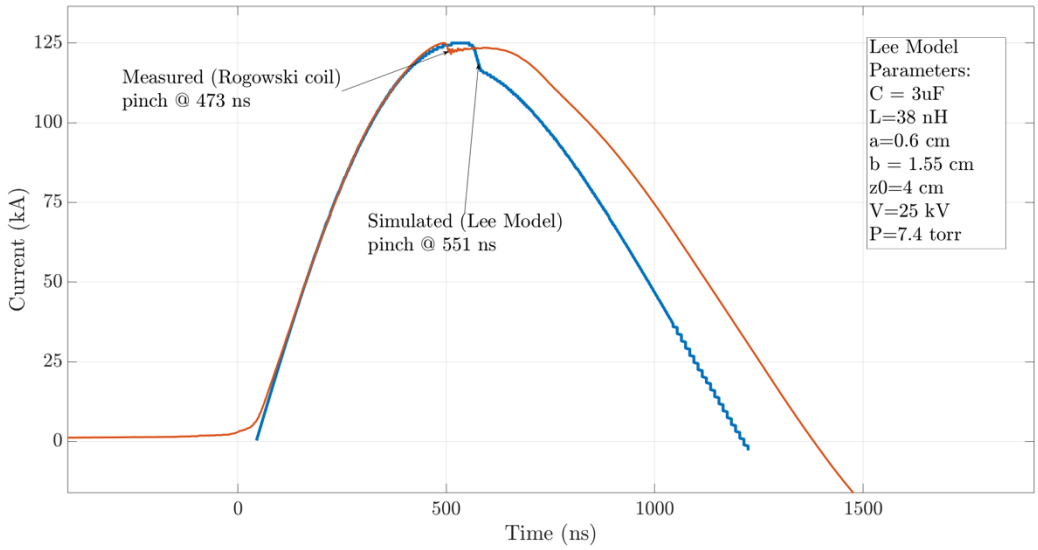

Figure 10. Current waveform as measured by Rogowski coil (orange) and as predicted by Lee Model simulation (blue)

Experiment Results

The portable DPF SNM measurement campaign was separated into two experimental phases. The first phase exercised the logistics and experimental methods in a low-risk, low-cost venue using materials with lower security and regulatory overhead (i.e., no highly enriched uranium [HEU] or plutonium [Pu]). We chose to use the Active Interrogation Building (AIB) at the NNSS's RNCTec facility because of its large, indoor experimental floor space and its ability to host portable radiation-generating devices (RGDs) and small quantities of depleted uranium (DU). The second phase of the experiment was to measure HEU active interrogation signals

using the portable DPF as a stimulating source at the DAF, which has significantly increased logistics complexity and expense. In both cases the experimental configuration was essentially identical; only the materials available to interrogate changed. Figure 11 shows the basic experimental configuration for both phases.

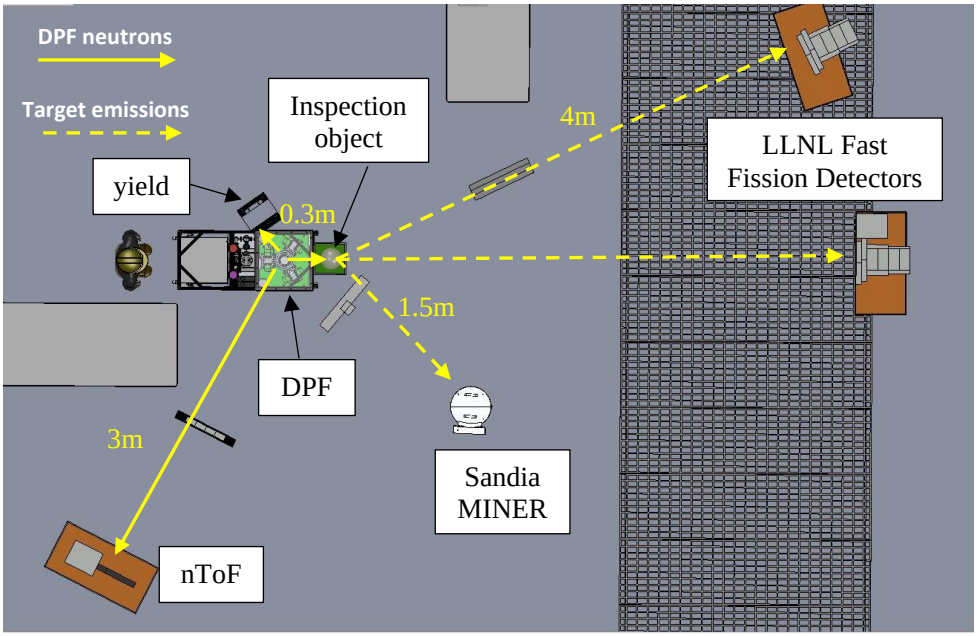

Figure 11. Experimental configuration for both phases of the portable DPF SNM measurement campaign

The configuration comprised three primary components: the DPF itself, the inspection object, and detectors. The DPF was operated in auto-fire mode in sequences of between 50 and 100 shots with approximately 30 seconds between each shot. The inspection object was placed about 30 cm from the DPF pinch, and the material was varied depending on the experimental facility (e.g., materials such as air, lead, and DU at RNCTec, and HEU, tungsten, and Pu at DAF). Detectors included DPF diagnostics such as the silver activation detector for neutron yield

measurement and the neutron time of flight detector and material sensing diagnostics including SNL's Mobile Imager of Neutrons for Emergency Responders (MINER) detector and LLNL's fast-fission detector system. The following sections detail specific results in each of the two phases of the campaign.

Phase One: RNCTec

The AIB at RNCTec is a large, indoor experimental facility that provided an ideal test bed for this experiment. Due to its nature, RNCTec could support the use of DU objects to provide preliminary fission data for the material sensing diagnostics. Two DU objects were interrogated, approximately 23.4 kg of DU plates covered in Plexiglas and approximately 50 kg of nested DU shells alloyed with titanium. Figure 12 shows both DU inspection objects. Approximately 173 shots were recorded on the DU plates and 30 shots were recorded on the DU shells. The DU shell investigation was unexpectedly cut short due to an insulator flashover that required a partial rebuild of the DPF acrylic insulator system, which could not be repaired in time to accumulate further data on the DU object at RNCTec.

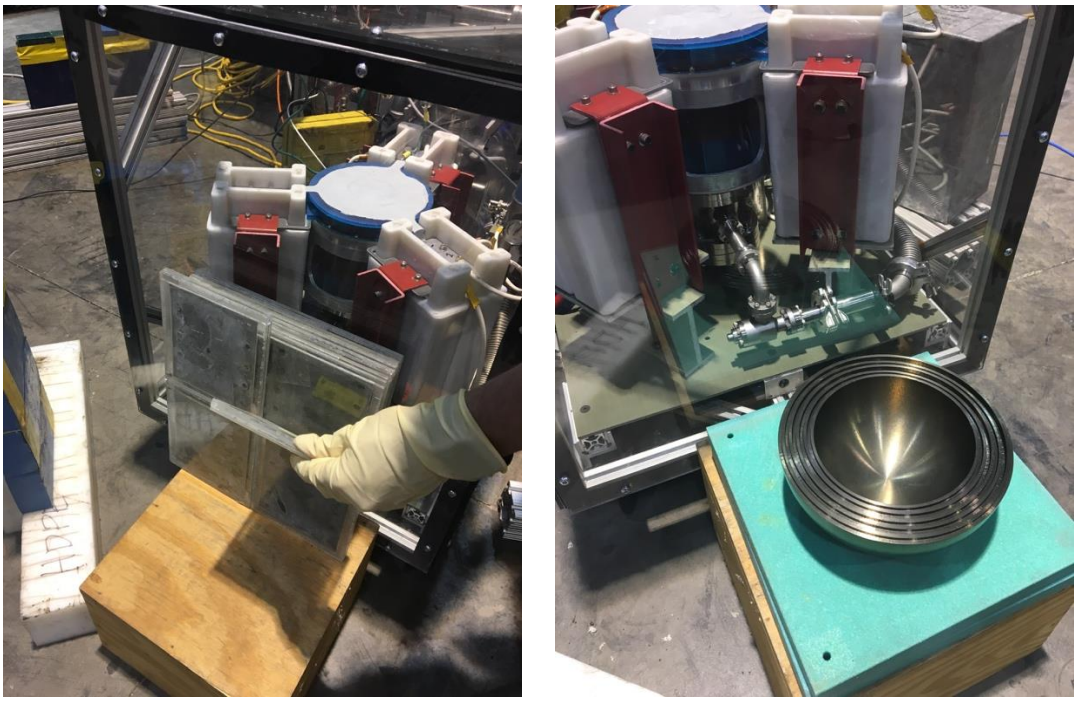

Figure 12. (left) DU plates covered in clear Plexiglas. (right) DU shells with top half removed to show concentric inner shells.

Collaborators from SNL fielded the MINER diagnostic system and performed data analysis on the measurements to interpret the results. MINER was originally developed for search and characterization of SNM through passive measurements in relatively low rate environments (Goldsmith 2014). The system uses a large volume of EJ-309 scintillator in the form of sixteen 3″ × 3″ cells. The double scatter interaction that allows MINER to image and measure neutron energy requires a single neutron to interact in two separate cells, and be time resolved through time-of-flight. This can pose a problem in high rate environments, as multiple cell interactions from different neutrons in a short time (tens of nanoseconds) can lead to pileup and incorrect event reconstruction.

A relatively short background run of 8.5 minutes will be compared to a 14 minute data acquisition where the portable DPF fired 20 shots. In addition, we have a long overnight (17.6 hours) acquisition of the DU without the DPF firing. The analysis is complicated due to pileup during the DPF operation which leads to multiple gammas appearing as false neutrons. Some of the pileup was improved by the trigger window code, but it was not entirely removed.

In the following figures, the left column shows the neutron image and energy spectrum, while the right shows the gamma energy and spectrum. Typically several hundred neutrons are necessary to build up an image with good statistics. Generally, when fewer neutrons than this are available, the image is unreliable; if many more neutrons are imaged and there is no hot spot, the source may not have a well-defined spatial distribution (such as background).

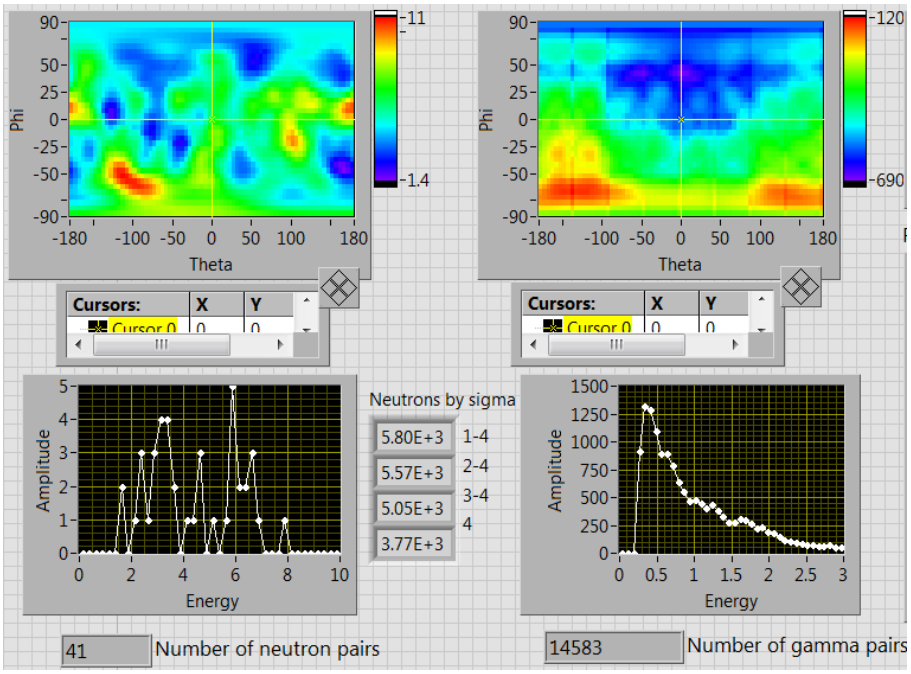

Figure 13. An 8.5-minute background acquisition, 41 total neutron pairs, 4.8 neutron pairs/minute

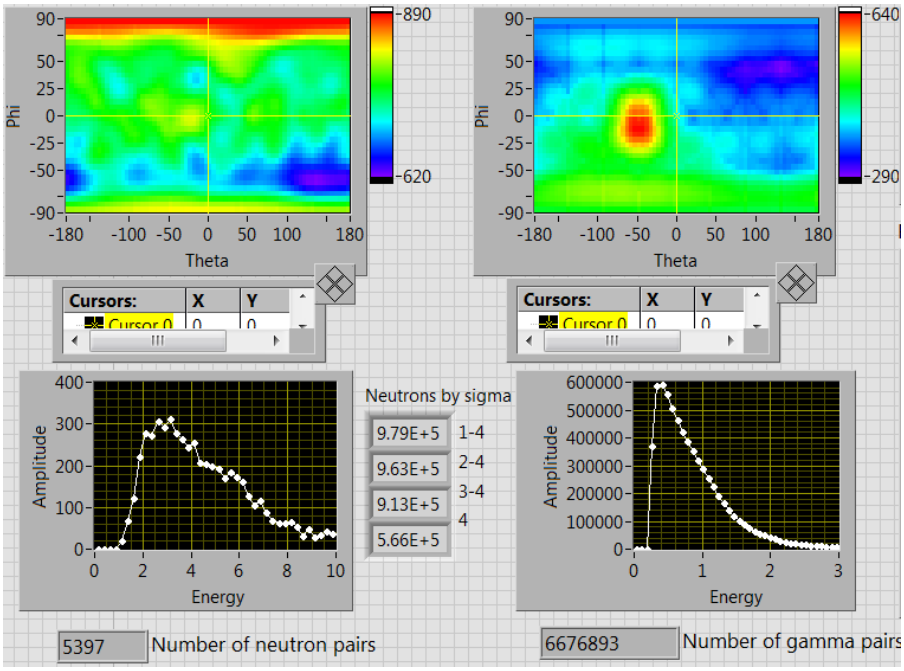

Figure 14. Long, 17.6-hour passive measurement of depleted uranium, 5,397 neutron pairs, 5.1 neutron pairs/minute

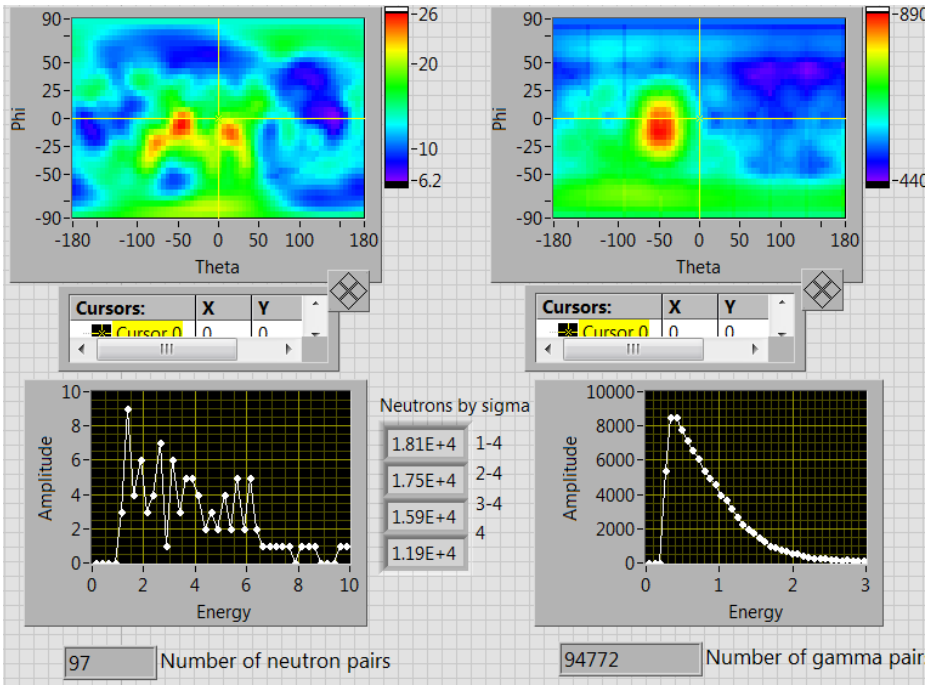

Figure 15. Depleted uranium, 20 shots, 97 neutron pairs, 6.9 neutrons/minute

Figure 15 does show a neutron hot spot roughly where we expect the target to be, but it is not well resolved; this could be due to the direct neutrons from the DPF. Because of this, and the fact that the simple analysis above shows the integration over the whole acquisition time, we investigated using post-processing windows after the initial flash of the DPF. We also observed pileup in the pulse shape discrimination. This problem persisted despite our efforts to define proper windows, leading us to conclude that further efforts would be required to manage pileup and a better understanding of the scattering environment and timing would be necessary.

After we adjusted the post processing windows to show only delayed events immediately after a shot, rates were drastically reduced. This result implies that hundreds of DPF shots would be required to build up our neutron image. MINER was not able to produce an active interrogation image of the depleted uranium in our measurement time using the windowed processing methods. Several factors could contribute to a better measurement, including better event processing/triggering, detector positioning, shielding, and a greater number of shots on the target.

Collaborators from LLNL modeled the setup using MCNP and deployed an experiment using their fast-fission diagnostic. The goal was to discover whether a short-pulse neutron interrogation system could be used to detect and differentiate fissionable materials. The diagnostics setup for this work is shown in Figure 16 for one example experiment.

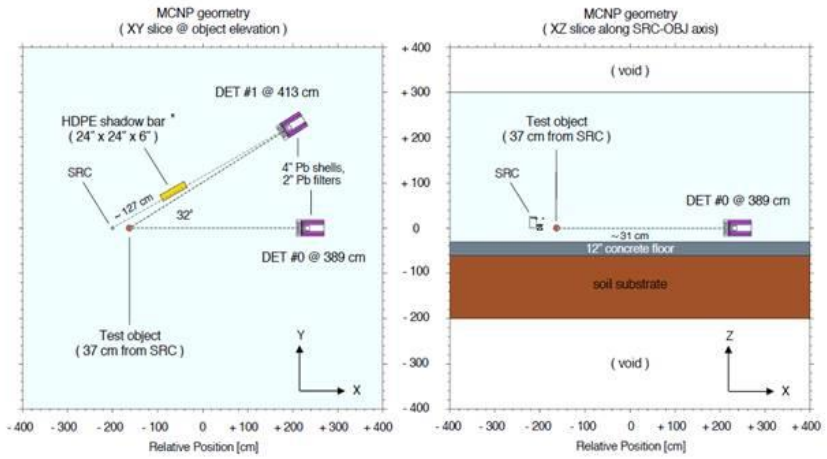

Figure 16. MCNP-modeled geometry of the source, object, and approximate detector setup

The goal of this work is to identify the fast fission neutrons that "outrun" the DPF source neutrons. This method was first tested at LLNL using an immobile 1 kJ scale system, where a signal was observed that supported the feasibility of this method (Podpaly 2018). In this work, we repeated Podpaly's experiment using the NNSS portable DPF system. Our doing so is a major step forward for deploying this detection scheme, and it provided independent confirmation of the method. An example expected neutron arrival signal with DU is shown in Figure 17.

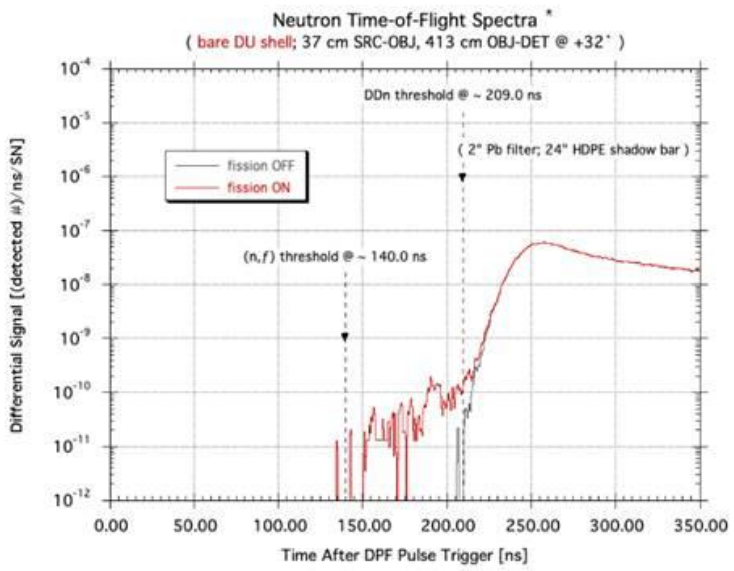

Figure 17. Example expected neutron signal from a DU shell with 2″ of lead

The early arrival signal depends on the distances from the source to the object and the object to the detector. In the case of DU for a DPF yield of 5×10^7 neutrons/pulse approximately a 20 kg DU target, we expect approximately 1/10 discharges to have early arrival signal. Example discharges are shown in Figures 18 and 19 with no object and a DU object, respectively. We did not observe any definite early arrival hits on the air shots, but there was some scatter in the rising edge of the neutron signal. Confident early arrival signals occurred on 7 of the 110 DU instead of the expected 11; however, there was significant self-shielding possible due to a differing geometry of the objects—plates instead of a DU sphere. These results are encouraging and consistent with the previous LLNL results, and comparison with HEU data from the experimental series is ongoing.

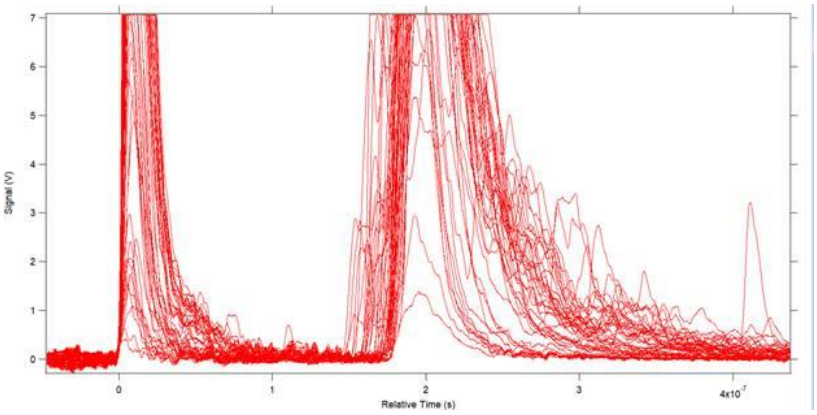

Figure 18. Overplot of DU discharges with no target in place. These data show 45 air discharges.

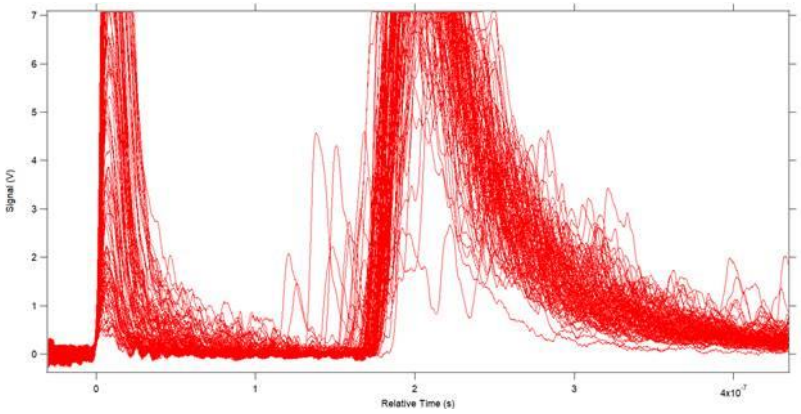

Figure 19. Overplot of DU discharges from RNCTec. Note signal arriving prior to bulk of the neutrons. These data show 110 DU discharges.

Phase Two: DAF

While the first phase of experiments at RNCTec went relatively smoothly, phase two work at the DAF posed several logistical hurdles that significantly reduced the quantity and quality of data collected. First, scheduling issues at the DAF pushed our window to conduct experiments out to near the project's end, which greatly reduced our ability to perform analysis or conduct follow-up experiments. Second, an oversight in the safety analysis process to admit new hardware into

DAF did not observe the machine's need for the deuterium fuel supply bottle. When this situation was noticed by the operational team, we were faced with designing a workaround. Only a slight technical modification would be required to solve this problem, but the aforementioned experiment delay did not allow enough time to implement it. This setback ultimately reduced the number of shots from an expected 3000 to approximately 100. Furthermore, our SNL collaborators were unable to support a second week of operations; thus, we were not able to accumulate any imaging data on SNM objects at DAF using MINER. Separately, while the LLNL fast-fission diagnostic worked well at RNCTec, two of the detectors are suspected to have been damaged in transit to the DAF or to have developed power issues in the facility, such that they were not functioning properly, which substantially reduced the fidelity of the measurement system. While preliminary analyses are suggestive of an effect from HEU, we do not currently have conclusive results. Nevertheless, the act of operating a DPF neutron generator inside of DAF in close proximity to SNM objects was a milestone accomplishment and represents a significant logistical achievement, paving the way for future measurements of this type. Figure 20 shows photographs of the portable DPF system inside DAF with an HEU and Pu inspection object.

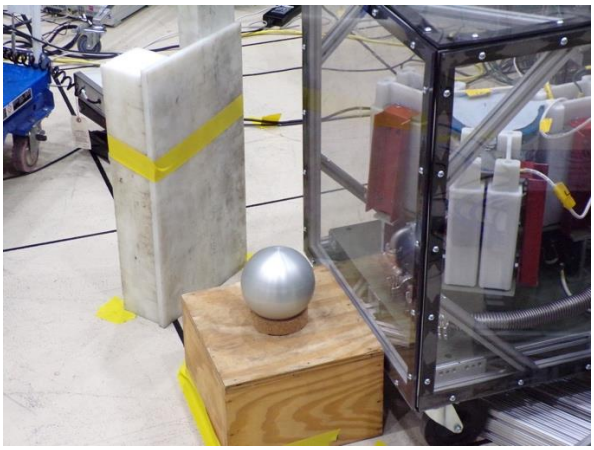

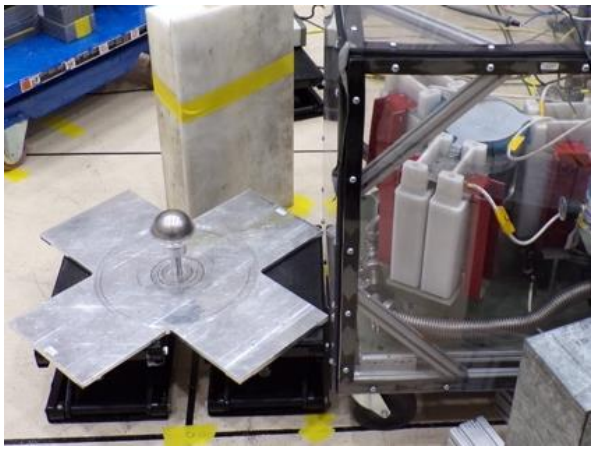

Figure 20. (left) Portable DPF with HEU inspection object at DAF. (right) Portable DPF with Pu inspection object at DAF.

Conclusion

A portable DPF system was designed, built, and tested to execute portable active interrogation measurements for nonproliferation applications to detect clandestine SNM. The DPF was transported to RNCTec and DAF at the NNSS to measure induced fission products from SNM objects and verify the DPF's ability to detect SNM. Partners from SNL and LLNL fielded detector platforms to measure induced fission products using the portable imaging system MINER and a newly developed fast fission detector array. Depleted uranium was detected with high certainty; however, logistical complications reduced the amount of data collected on HEU. These complications included repeated delays in access to the DAF facility and the inability to operate a deuterium gas supply bottle inside DAF. Despite these issues, the DPF was fired successfully more than 100 times on an HEU object, and the fast-fission diagnostic may have detected fission products. This effort signifies several milestone achievements, not only within this SDRD project itself, but within the broader nuclear security enterprise. This project was a collaboration among all three weapons labs and the NNSS; furthermore, it was the first time SDRD or the M&O have functioned as a customer to DAF, it was the first time that a DPF has been brought into DAF and operated for neutron production, and it was the first attempted measurement on plutonium by a DPF.

The portable DPF system had an average neutron yield of 5.84×10^7 neutrons per pulse with a repetition rate of 30 seconds, providing a time average neutron yield of 1.95×10^6 neutrons per

second, which is approximately two times higher than the required output to accomplish portable active interrogation missions. Only slight modifications are required to increase the repetition rate to two shots per second, which will increase the output rate to above 10^8 neutrons per second, and other improvements to the pulsed-power bank and plasma process chamber will increase the per-shot yield even further. The size of the portable DPF system can be greatly reduced by shrinking the control system down to PCB components and by eliminating the vacuum chamber, enabling a truly field-compatible form factor. Finally, the fusion fuel can be readily converted to a deuterium–tritium mix to provide up to an 80 times increase in neutron production at the enhanced neutron energy of 14.1 MeV.

Significance

While portable neutron generators have been used for mobile active interrogation applications, none have used dense plasma focus techniques for neutron production. This work is the first successful active interrogation measurement of SNM using a person-portable DPF system, which has advantages over conventional commercial neutron sources including increased neutron output, greatly reduced pulse-width, and reduced complexity.

Tie to Mission/Benefit

This work contributed to mission success by delivering a novel active interrogation tool to the NNSS and its partners. This achievement augments our nation's ability to protect against the threat of clandestine nuclear material by providing an effective, easily transportable instrument to detect SNM in a variety of key settings such as border crossings, ports of entry, combat and emergency response scenarios, and urban environments.

Publications, Technology Abstracts

This work was presented at three conferences including 2018 IEEE International Conference on Plasma Science, 2019 Pulsed Power and Plasma Science Conference, and 2019 Pacific Symposium on Pulsed Power Applications.

TRL Start and End

At the start of this project was approximately TRL 1, with the basic principles established. As a company, we had extensive experience with large-scale DPF systems, which provided a framework for the fundamental physics of the DPF process, yet we had no experience with the engineering techniques required to scale down to a portable form factor. At the end of this project, the technology is TRL 6, with a prototype system demonstrated. Our work at RNCTec and DAF demonstrated that a DPF could be used to detect SNM objects. Now we must refine our detection modality and make the above-mentioned improvements to further improve the DPF neutron output and ease of use.

Acknowledgments

The team would like to thank Stephen Molnar for greatly assisting with design and construction, E. Chris Hagen for project planning guidance; Al Mitlyng for diligently working to procure components; Gladys Arias-Tapar for designing an RGD registration plan and work package for this project; Larry Platte, Greg Doyle, and Lyle Warren for coordinating our operations at RNCTec; and M. Krishnan for welcoming our team to his laboratory, AASC in San Leadro, California, to learn about compact DPF design techniques.

This work was performed under the auspices of the U.S. Department of Energy by Lawrence Livermore National Laboratory under Contract DE-AC52-07NA27344 and were supported by the LLNL-LDRD Program under Project No. 19-FS-034.

This manuscript has been authored by Mission Support and Test Services, LLC, under Contract No. DE-NA0003624 with the U.S. Department of Energy, National Nuclear Security Administration, Office of Defense Programs and supported by the Site-Directed Research and Development Program. The United States Government retains and the publisher, by accepting the article for publication, acknowledges that the United States Government retains a non-exclusive, paid-up, irrevocable, worldwide license to publish or reproduce the published form of this manuscript, or allow others to do so, for United States Government purposes. The U.S. Department of Energy will provide public access to these results of federally sponsored research in accordance with the DOE Public Access Plan (http://energy.gov/downloads/doe-public-access-plan). The views expressed in the article do not necessarily represent the views of the U.S. Department of Energy or the United States Government. DOE/NV/03624--0999.

References

Bernard, A., P. Cloth, H. Conrads, A. Coudeville, G. Gourlan, A. Jolas, C. Maisonnier, J. P. Rager. 1977. “The dense plasma focus — A high intensity neutron source.” *Nucl. Instrum. Methods* **145** (1): 191–218. https://doi.org/10.1016/0029-554X(77)90569-9.

Gall, B., N. Bennett, T. Meehan, M. Heika, M. Blasco, V. DiPuccio, J. Bellow, A. Wolverton, J. Tinsley, R. O’Brien. 2018. “Man-portable dense plasma focus for neutron interrogation

applications." In *FY 2017 Site-Directed Research and Development Annual Report*, 79–90. Las Vegas, Nevada: Mission Support and Test Services, LLC.

Gall, B., M. Heika, M. Blasco, J. Bellow, B. T. Meehan, V. DiPuccio, A. Wolverton, J. Tinsley, N. Bennett. 2019. "Man-portable dense plasma focus for neutron interrogation applications." In *FY 2018 Site-Directed Research and Development Annual Report*, 91–100. Las Vegas, Nevada: Mission Support and Test Services, LLC.

Goldsmith, J., J. Brennan, M. Gerling, S. Kiff, N. Mascarenhas, J. Van de Vreugde. 2014. "MINER – A Mobile Imager of Neutrons for Emergency Responders." SAND2014-19365R. Albuquerque, New Mexico: Sandia National Laboratories. https://prod-ng.sandia.gov/techlib-noauth/access-control.cgi/2014/1419365r.pdf.

Gribkov, V., A. Dubrovsky, L. Karpiski, R. Miklaszewski, M. Paduch, M. Scholz, P. Strzyewski, K. Tomaszewski. 2006. "The Dense Plasma Focus Opportunities in Detection of Hidden Objects by Using Nanosecond Impulse Neutron Inspection System (NINIS)." In *AIP Conference Proceedings* **875**: 415. https://doi.org/10.1063/1.2405977.

Hussain, S., S. Ahmad, M. Z. Khan, M. Zakaullah, A. Waheed. 2003. "Plasma focus as a high intesity flash x-ray source for biological radiography." *J. Fusion Energy* **22**: 195–200. https://doi.org/10.1023/B:JOFE.0000037787.36243.b1.

Krishnan, M. 2012. “The dense plasma focus: A versatile dense pinch for diverse applications.” *IEEE Trans. Plasma Sci.* **40** (12): 3198–3221. https://ieeexplore.ieee.org/document/6341852.

Lanter, R. J., D. E. Bannerman. 1968. “Silver counter for bursts of neutrons.” *Rev. Sci. Instrum.* **39**: 1588. https://doi.org/10.1063/1.1683178.

Lee, S., P. Lee, G. Zhang, X. Feng, V. A. Gribkov, M. Liu, A. Serban, T. K. S. Wong, 1998. “High rep rate high performance plasma focus as a powerful radiation source.” *IEEE Trans. Plasma Sci*. **26** (4): 1119–1126. https://www.researchgate.net/publication/239612502_High_rep_rate_high_performance_plasma_focus_as_a_powerful_radiation_source.

Lee, S. 2014. “Plasma focus radiative model: Review of the Lee Model code.” *J. Fusion Energy* **33**: 319–335.

Mather, J. W. 1964. “Investigation of the high-energy acceleration mode in the coaxial gun.” *Phys. Fluids* **7** (11): S28–S34. https://doi.org/10.1063/1.1711086.

Mather, J. W. 1965. “Formation of a high-density deuterium plasma focus.” *Phys. Fluids* **8** (2): 366–377.

Niranjan, R., R. K. Rout, R. Srivastava, T. C. Kaushik, S. C. Gupta. 2016. *Rev. Sci. Instrum*. **87** (3): 033504. https://doi.org/10.1063/1.4942666.

Office of Defense Nuclear Nonproliferation (NA-22), "DNN R&D Call for Proposals." 2018.

Podpaly, Y. A., et al. 2018. "Environment Insensitive Detection of Fissionable Material with a Short Pulse Neutron Source." IAEA-CN-269-363. Paper presented at the International Conference on the Security of Radioactive Material: The Way Forward for Prevention and Detection, Vienna, Austria.

Rawat, R. S. 2013. "High-energy-density pinch plasma: A unique nonconventional tool for plasma nanotechnology." *IEEE Trans. Plasma Sci.* **41** (4): 701–715. https://ieeexplore.ieee.org/document/6407693.

Rapezzi, L., M. Angelone, M. Pillon, M. Rapisarda, E. Rossi, M. Samuelli, F. Mezzetti. 2004. "Development of a mobile and repetitive plasma focus." *Plasma Sources Sci. Technol.* **13** (2): 272–277. https://iopscience.iop.org/article/10.1088/0963-0252/13/2/011.

Shukla, R., A. Shyam, R. Verma, E. Mishra, M. Meena, K. Sagar, P. Dhang. 2015. "Results of ultracompact plasma focus operating in repetitive burst-mode." *IEEE Trans. Plasma Sci.* **43** (8): 2354–2358. https://ieeexplore.ieee.org/document/7151848.

Welch, D., D. Rose, B. Oliver, R. Clark. 2001. "Simulation techniques for heavy ion fusion chamber transport." *Nucl. Instrum. Methods Phys. Res. A* **464**: 134–139. https://doi.org/10.1016/S0168-9002(01)00024-9.

Zhang, T., J. Lin, A. Patran, D. Wong, S. M. Hassan, S. Mahmood, T. White, T. L. Tan, S. V. Springham, S. Lee, P. Lee, R. S. Rawat. 2007. “Optimization of a plasma focus device as an electron beam source for thin film deposition.” *Plasma Sources Sci. Technol.* **16** (2): 250–256. https://iopscience.iop.org/article/10.1088/0963-0252/16/2/006.